applied sciences

MDPI

Article

Ultra-Broadband Bending Beam and Bottle Beam Based on Acoustic Metamaterials

Xudong Fan, Xiaolong Huang, Yang Kang, Can Li, Ning Li * and Chunsheng Weng *

National Key Laboratory of Transient Physics, Nanjing University of Science and Technology, Nanjing 210094, China; fanxudong@njust.edu.cn (X.F.); huang_xl@njust.edu.cn (X.H.); ykang@njust.edu.cn (Y.K.); lican@njust.edu.cn (C.L.)

* Correspondence: lining@njust.edu.cn (N.L.); weng@njust.edu.cn (C.W.)

Abstract: We report the realization of an ultra-broadband bending beam based on acoustic metamaterials by the theoretical prediction and the numerical validation. The proposed structure is composed of a series of straight tubes with spatially modulated depths. We analytically derive the depth profile required for the generation of an ultra-broadband bending beam, and examine the performance of the metastructure numerically. The design is then extended for the generation of a three-dimensional bottle beam. The transverse trapping behaviours on small rigid objects by the bottle beam are investigated based on the force potential. Our work will help the further study of broadband acoustic meta-structures, and may also find applications in a variety of fields such as ultrasound imaging, health monitoring and particle manipulations.

Keywords: acoustic metamaterials; bending beams; bottle beams; particle manipulations

Citation: Fan, X.; Huang, X.; Kang, Y.; Li, C.; Li, N.; Weng, C. Ultra-Broadband Bending Beam and Bottle Beam Based on Acoustic Metamaterials. *Appl. Sci.* **2022**, *12*, 3025. https://doi.org/10.3390/app12063025

Academic Editors: Xiaojun Liu, Zhiwang Zhang and Jiuyang Lu

Received: 17 February 2022
Accepted: 15 March 2022
Published: 16 March 2022

1. Introduction

The precise manipulation of acoustic waves based on acoustic materials is critical in the fundamental research in acoustics, and also plays a significantly important role in the fields of medical imaging, ultrasound therapy, acoustic detection and communications. Compared with the conventional speaker array systems possessing the bulkier array size and complex signal processing algorithm, precise manipulations of sound fields based on the smaller passive artificial structures have attracted enormous interests. With the extraordinary features and properties, these artificial structures, called acoustic metamaterials, Ref. [1] can be used to steer sound waves in a flexible and controllable way. Refs. [2–28] Various novel phenomena have been achieved with the aid of acoustic metamaterials, such as negative refraction or reflection, Refs. [29–31], acoustic one-way propagation, Ref. [32] acoustic cloaking, Refs. [33–38], acoustic hologram, Refs. [39,40] and vortex field generation. Ref. [41] The recent development of acoustic meta-gratings [42–48] and meta-clusters [49] provides a novel perspective in regard of the passive control of waves based on acoustic metamaterials. Latterly, the incorporation of the artificial intelligence techniques and machine learning methods into the inverse design of acoustic metamaterials also suggests an innovative way for the design of relevant acoustic devices involving the field manipulations. Refs. [50–57] Despite the great success achieved by the acoustic metamaterials in the manipulations of acoustic fields, most of the previous structures suffer from the unavoidable narrow-band problem due to the local resonance mechanism, which, in a certain sense, limits the applications of these structures in the practical situations. Hence, it would be highly desired to explore the acoustic metamaterials for the field manipulations within a broad band at different frequencies.

In this paper, we propose to design a reflected acoustic metastructure to effectively generate a bending beam within an ultra-broad frequency range. The structure is simply composed of a series of straight tubes with different depths, and the depth is modulated based on the spatial location of each tube. The depth profile of the structure for the bending

beam is analytically derived, and it is proved that the depth profile does not explicitly depend on the wavelength, suggesting the possibility to realize the bending beam in a broad band. The performance of the designed reflective structure is examined numerically and then extended to three-dimensional situations for the generation of a bottle beam. The acoustic trapping behaviours on small rigid objects by the bottle beam are analyzed based on the force potential. With the simple design and great performance, the metastructure proposed here may find applications of acoustic devices involving the field manipulations. Our work also suggests the particle manipulations with the aid of acoustic metamaterials.

2. Materials and Methods

We will first explain the design of the acoustic meta-structure for ultra-broadband bending beams. The structure consists of an array of straight tubes with different spatially modulated depths h (Figure 1). [6] Each tube of the structure has an identical width much smaller than the working wavelength, i.e., $w << \lambda$ with w and λ being the width of the tubes and the working wavelength, respectively, (see Inset in Figure 1). In addition, the wall of each tube is designed to be sufficiently thin to avoid the impedance mismatch between the structure and the background medium (the thickness of the wall is $0.1p$ with p being the period of the structure). Hence, the incident sound waves can easily enter the tubes with little reflections on the interface. After the reflection by the bottom of each tube, the reflected sound wave will possess a depth-dependent phase shift, i.e., $\phi = k \times (2h)$, with $k = 2\pi/\lambda$ being the wavenumber. Consequently, the desired phase profile on the interface of the structure can be achieved by carefully engineering the depth profile of the tubes, which suggests the ability to generate a ultra-broadband bending beam desired here.

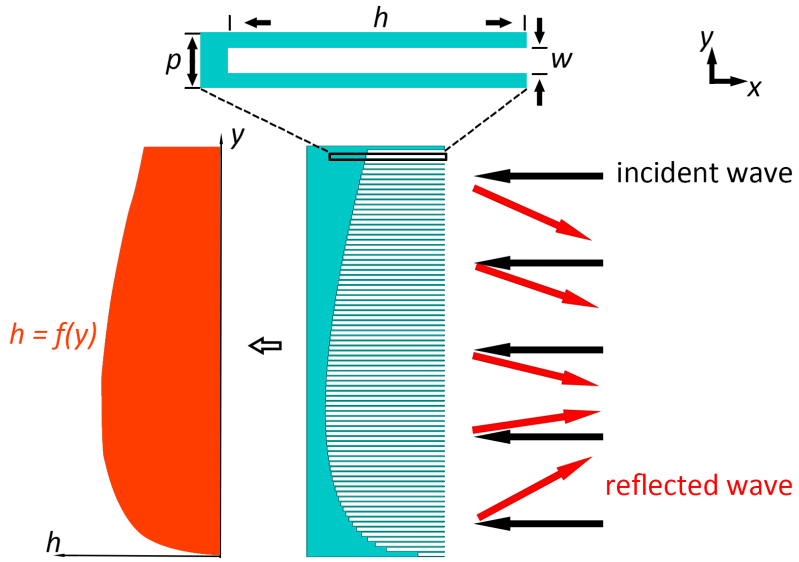

Figure 1. Illustration of the ultra broadband structure. Black arrows: incident waves; red arrows: reflected waves. Inset: zoom-in plot of a single tube within the structure. The depth profile of the tubes, h, is a function of the spatial location y. $p = \lambda/8$ is the period of the structure, and $w = 0.8p$ is the width of each tube.

In the current study, the the proposed scheme will be utilized to generate an ultra-broadband bending beam (Figure 1). To realize an arbitrary bending trajectory $y = f(x)$, the phase profile can be expressed as [3]

$$\frac{d\phi(y)}{dy} = -k_0 \sin\theta_r = -k_0 \frac{f'(x)}{\sqrt{1 + [f'(x)]^2}} \tag{1}$$

where $f'(x) = \tan\theta_r$ is the slope of the trajectory with θ_r being the reflected angle. For a half circular trajectory $f(x) = \sqrt{R^2 - (x - R)^2}$ with the center at $(x, y) = (R, 0)$, the

desired phase profile can be obtained as $\phi(y) = -k_0(y - 2R\sqrt{y/R})$, and then the depth profile of the tube can be simply expressed as:

$$h(y) = C - (y/2 - R\sqrt{y/R}), \tag{2}$$

where a positive number C is used to make sure the depth of each tube, $h(y)$, is non-negative. It is worth mentioning that the depth profile of the tubes in Equation (2) does not explicitly rely on the working frequency or the wavelength, suggesting the possibility to achieve a bending beam in a broad band of different frequencies with the same structure.

Here, the numerical simulations for bending beams were conducted in the two-dimensional pressure acoustic module using the commercial software, COMSOL MULTIPHYSICS; see Figure 2 for the sketch of the numerical setup. The size of the computation domain is 1.8 m $\times$ 1.8 m. Radiation boundaries were applied to the outer boundaries of the computation domain to eliminate the reflection. The whole length of the structure is 1m, and the period of the structure is $p = 1.2$ cm. Maximum mesh size was set to be $\lambda/20$ so as to obtain the precise and accurate sound fields. The background medium is air with the density of 1.21 kg/m^3 and the sound speed of 343 m/s. For the simulations with the acoustic meta-structure (considered to be rigid) (Figure 2a), the background pressure field was used as the source to generate an incident plane wave propagating along the $-x$ direction, and the scattered fields were examined to check the performance. However, for the simulation with the ideal source (Figure 2b), the source is located at $x = 0$ to generate the ideal bending field directly.

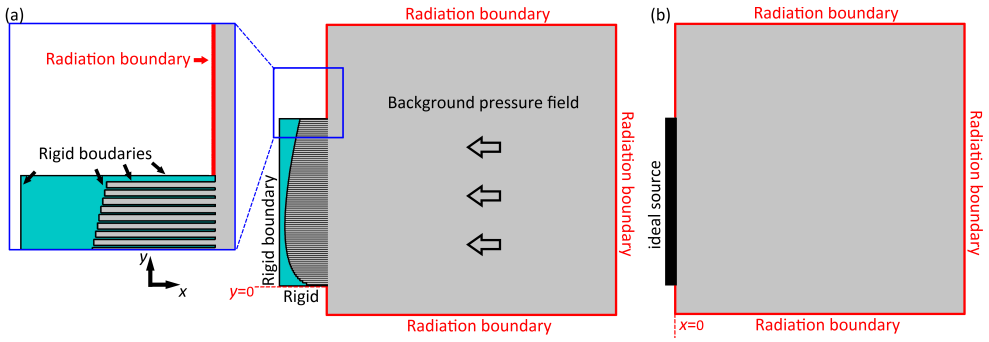

Figure 2. Sketch of the numerical setup for the simulations with (**a**) the metastructure and (**b**) the ideal source. Radiation boundaries (red solid lines) are applied to the outer boundaries of the computation domain, whose size is 1.8 m $\times$ 1.8 m. (**a**) Boundaries of the metastructure are set to be rigid (black solid lines). Background pressure field (gray) is used to generate an incident plane wave propagating along $-x$ direction. Inset: zoom-in plot in the region marked by the blue box. (**b**) Black solid rectangular indicates the ideal source to generate the ideal bending field directly.

The simulations for the three-dimensional bottle beams were conducted with the same parameters as mentioned above but in a two-dimensional symmetry model with $y = 0$ being the symmetrical axis. The force potential U was computed based on the simulated pressure and velocity fields [58], i.e.,

$$U = (\pi a^3/3)[f_1 p^2/(\rho_0 c_0^2) - (3/2) f_2 \rho_0 \mathbf{v}^2], \tag{3}$$

where a is the radius of the object, ρ_0 and c_0 are the mass density and the sound speed of the background medium, and f_1 and f_2 are the monopole and dipole factors depending on the mass density ratio and bulk modulus ratio between the object and the surrounding medium [59,60]. Here, rigid particles with $f_1 = 1 = f_2$ were used in the calculation since for most solid objects, the density and bulk modulus are much larger than the background medium, air, so the results here are applicable to most elastic objects.

3. Results

3.1. Bending Beams

As an example, we present the generation of a bending beam with the radius $R = 0.35$ m. With the aid of the expressions of the phase $\phi(y)$ and the depth $h(y)$ mentioned above, the desired phase profile and corresponding depth profile for the bending beam can be obtained, as shown in Figure 3a,b, respectively. The depth profile in Figure 3b has been discretized based on the period p of the metastructure so that each dot in (b) shows the depth of the corresponding tube within the structure shown in Figure 3c. The structure will be used to generate the bending beam. We have simulated the reflected fields $|p|^2$ by the metastructure shown in Figure 3c for different frequencies; see top panels in Figure 4. The bending beams are successfully generated within a broadband frequency range (2 kHz to 17 kHz) by the same structure. The results are then compared with the fields generated by an ideal source of the same size; see bottom panels. From the results, the fields generated by the metastructure agree well with the fields generated by the ideal source, whose phase profile is shown in Figure 3a.

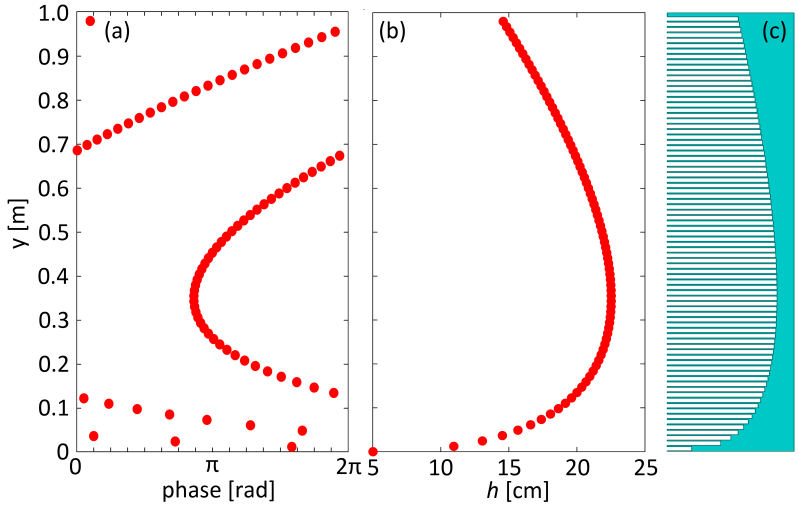

Figure 3. Desired parameters for the generation of bending beams. (**a**) The phase profile at the interface of the structure for the bending beam with $R = 0.35$ m, and (**b**) the corresponding depth profile for the bending beam (see Equation (2)). (**c**) The metastructure is designed based on the depth profile in (**b**).

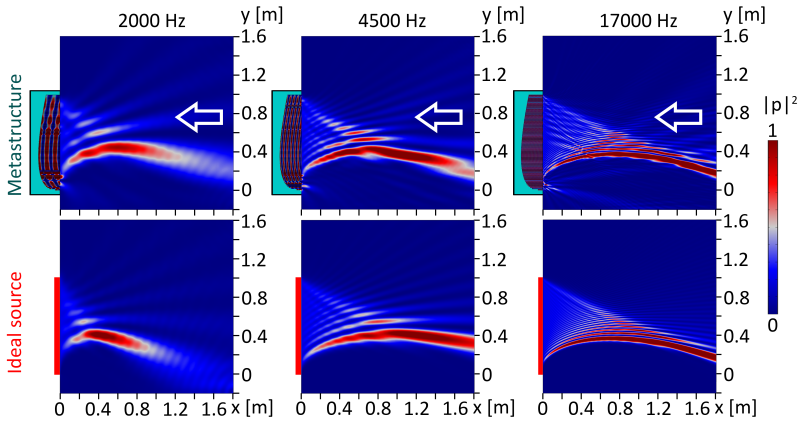

Figure 4. Simulated bending fields. (**Top** panels) bending beams generated by the metastructure at the frequencies: 2000, 4500 and 17,000 Hz; (**Bottom** panels) bending beams generated by an ideal source for comparison. White arrows indicate the incident plane waves.

3.2. Bottle Beam and Particle Manipulations

The design for the bending beams are then extended for the generation of a three-dimensional bottle beam by rotating the metastructure in Figure 3c along $y = 0$ axis. The simulated three-dimensional sound field for the bottle beam at 3500 Hz is shown in Figure 5a. From the result, the sound waves propagate along a curved path, and eventually form a focal point. There exists a local 'empty' bottle inside the beam, where the sound intensity is almost zero. The sound field profile $|p|^2$ along the central z axis is shown in Figure 5b, where the pressure remains near 0 for quite a long distance ($\sim 20\lambda$). The pressure maximum happens at $z \approx 25.5\lambda$, and the focal length, obtained by the -3 dB locations (marked by two vertical red dashed lines), is about 3.7λ.

We further examine the field distribution along the transverse direction $r = \sqrt{x^2 + y^2}$ at $z \approx 5\lambda$ (black solid line in Figure 5c), where the diameter of the 'empty' region is about 7λ (see inset for the two-dimensional field at $x - y$ cross section). The corresponding force potential (Equation (3)) for small rigid particles is computed based on the simulated field, and the particles will be trapped to the potential minimum [red dots in Figure 5c]. From the results, the location to trap the particles is near the first peak of the pressure maximum. The field distribution and force profile near the focal point ($z \approx 25.5\lambda$) are also examined (Figure 5d). In this case, the particles cannot be trapped to the focal point (pressure maximum) at the center but at a location near the center where $r \approx 0.4\lambda$.

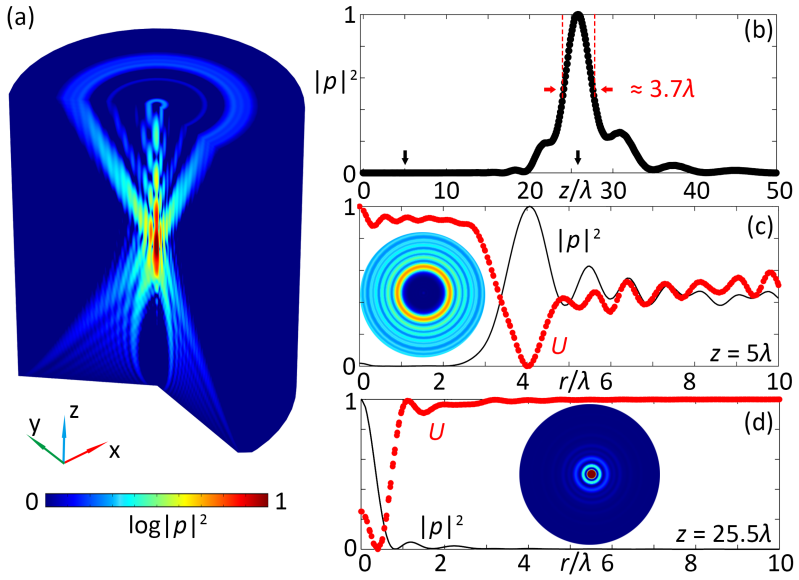

Figure 5. Particle manipulation based on the bottle sound beam. (**a**) Simulated three-dimensional bottle sound beam. (**b**) Normalized sound field $|p|^2$ profile along the central beam axis. Normalized sound fields $|p|^2$ and the force potential U in the transverse direction at (**c**) $z \approx 5\lambda$ and (**d**) $z \approx 25.5\lambda$. Insets: corresponding two-dimensional sound fields of $x - y$ cross section.

4. Discussion

In summary, we have designed a reflected metastructure, simply composed of an array of straight tubes with different spatially modulated depths, to generate a bending beam for sound within an ultra-broad band. The simulated fields via the acoustic metastructure agree well with the theoretical predictions as well as the fields generated by the ideal source. The design has also been extended for the generation of a three-dimensional bottle beam. The transverse trapping behaviours on small rigid objects by the bottle beam have been analyzed with the aid of the force potential. Our work will help the design and the development of broadband acoustic devices involving sound field manipulations, and also suggest the possibility to realize the precise particle manipulations along a curved trajectory.

The metastructure proposed here has exhibited the performance of the generation of bending beams with the broadband feature in the audible frequency range. It is worth

noting that the upper frequency limit could still be extended by reducing the width of each straight tube w so as to increase the cut-off frequency $f_0 = c_0/(2w)$ with w and c_0 being the tube width and the background sound speed, respectively. The computation cost will increase for higher frequencies due to the smaller wavelengths and the smaller mesh size required for the simulations based on the finite element methods. When the frequency is too high, for example in the ultrasound frequency range, the thermoviscous effect caused by the structure needs to be considered by including the acoustic boundary layers during the calculation using the thermoviscous acoustic module. However, it might be difficult for the fabrication of the structure since the width of each individual tube is much smaller than the wavelength, and the wavelength is on the scale of millimeters. On the other hand, the applications on low frequencies would be easier because the lower frequency limit could be simply extended by increasing the whole length of the structure along the interface direction (y direction) so as to make sure the whole size of the metastructure is comparable to the working wavelength.

Author Contributions: Conceptualization, X.F.; methodology, X.F.; software, X.F.; validation, X.F., N.L.; investigation, X.F., X.H., Y.K. and C.L.; writing–original draft preparation, X.F.; writing–review and editing, X.F., N.L., X.H., Y.K., C.L., C.W.; visualization, X.F., N.L., C.W.; supervision, N.L., C.W. All authors have read and agreed to the published version of the manuscript.

Funding: This research was funded by the Funds of the National Key Laboratory of Transient Physics (Grant No. 6142604200202), the Young Scientists Found of the Natural Science Foundation of Jiangsu Province (Grant No. BK20190439) and the Fundamental Research Funds for the Central Universities of Ministry of Education of China (Grant No. 30919011258).

Institutional Review Board Statement: Not applicable.

Informed Consent Statement: Not applicable.

Data Availability Statement: Not applicable.

Acknowledgments: The support from Ying Tao is acknowledged.

Conflicts of Interest: The authors declare no conflict of interest. The funders had no role in the design of the study; in the collection, analyses, or interpretation of data; in the writing of the manuscript, or in the decision to publish the results.

References

1. Liu, Z.; Zhang, X.; Mao, Y.; Zhu, Y.Y.; Yang, Z.; Chan, C.T.; Sheng, P. Locally Resonant Sonic Materials. *Science* **2000**, *289*, 1734–1736. [CrossRef] [PubMed]
2. Zhang, P.; Li, T.; Zhu, J.; Zhu, X.; Yang, S.; Wang, Y.; Yin, X.; Zhang, X. Generation of acoustic self-bending and bottle beams by phase engineering. *Nat. Commun.* **2014**, *5*, 4316. [CrossRef]
3. Li, Y.; Jiang, X.; Li, R.Q.; Liang, B.; Zou, X.Y.; Yin, L.L.; Cheng, J.C. Experimental realization of full control of reflected waves with subwavelength acoustic metasurfaces. *Phys. Rev. Appl.* **2014**, *2*, 064002. [CrossRef]
4. Tang, K.; Qiu, C.; Ke, M.; Lu, J.; Ye, Y.; Liu, Z. Anomalous refraction of airborne sound through ultrathin metasurfaces. *Sci. Rep.* **2014**, *4*, 6517. [CrossRef]
5. Xie, Y.; Wang, W.; Chen, H.; Konneker, A.; Popa, B.I.; Cummer, S.A. Wavefront modulation and subwavelength diffractive acoustics with an acoustic metasurface. *Nat. Commun.* **2014**, *5*, 5553. [CrossRef] [PubMed]
6. Zhu, Y.F.; Zou, X.Y.; Li, R.Q.; Jiang, X.; Tu, J.; Liang, B.; Cheng, J.C. Dispersionless manipulation of reflected acoustic wavefront by subwavelength corrugated surface. *Sci. Rep.* **2015**, *5*, 0966. [CrossRef] [PubMed]
7. Li, Y.; Jiang, X.; Liang, B.; Cheng, J.C.; Zhang, L. Metascreen-based acoustic passive phased array. *Phys. Rev. Appl.* **2015**, *4*, 024003. [CrossRef]
8. Ma, G.; Sheng, P. Acoustic metamaterials: From local resonances to broad horizons. *Sci. Adv.* **2016**, *2*, e1501595. [CrossRef] [PubMed]
9. Cummer, S.A.; Christensen, J.; Alù, A. Controlling sound with acoustic metamaterials. *Nat. Rev. Mater.* **2016**, *1*, 1–13. [CrossRef]
10. Zhu, X.; Li, K.; Zhang, P.; Zhu, J.; Zhang, J.; Tian, C.; Liu, S. Implementation of dispersion-free slow acoustic wave propagation and phase engineering with helical-structured metamaterials. *Nat. Commun.* **2016**, *7*, 11731. [CrossRef] [PubMed]
11. Fan, X.D.; Zhu, Y.F.; Liang, B.; Yang, J.; Cheng, J.C. Broadband convergence of acoustic energy with binary reflected phases on planar surface. *Appl. Phys. Lett.* **2016**, *109*, 243501. [CrossRef]

12. Zhu, Y.; Fan, X.; Liang, B.; Cheng, J.; Jing, Y. Ultrathin acoustic metasurface-based Schroeder diffuser. *Phys. Rev. X* **2017**, *7*, 021034. [CrossRef]
13. Assouar, B.; Liang, B.; Wu, Y.; Li, Y.; Cheng, J.C.; Jing, Y. Acoustic metasurfaces. *Nat. Rev. Mater.* **2018**, *3*, 460–472. [CrossRef]
14. Fan, X.D.; Liang, B.; Yang, J.; Cheng, J.C. Illusion for airborne sound source by a closed layer with subwavelength thickness. *Sci. Rep.* **2019**, *9*, 1750. [CrossRef]
15. Fan, X.D.; Zhang, L. Acoustic orbital angular momentum Hall effect and realization using a metasurface. *Phys. Rev. Res.* **2021**, *3*, 013251. [CrossRef]
16. Chen, Z.; Peng, Y.; Li, H.; Liu, J.; Ding, Y.; Liang, B.; Zhu, X.F.; Lu, Y.; Cheng, J.; Alù, A. Efficient nonreciprocal mode transitions in spatiotemporally modulated acoustic metamaterials. *Sci. Adv.* **2021**, *7*, eabj1198. [CrossRef]
17. Li, J.; Wen, X.; Sheng, P. Acoustic metamaterials. *J. Appl. Phys.* **2021**, *129*, 171103. [CrossRef]
18. Zhang, C.; Cao, W.K.; Wu, L.T.; Ke, J.C.; Jing, Y.; Cui, T.J.; Cheng, Q. A reconfigurable active acoustic metalens. *Appl. Phys. Lett.* **2021**, *118*, 133502. [CrossRef]
19. Gu, Z.; Fang, X.; Liu, T.; Gao, H.; Liang, S.; Li, Y.; Liang, B.; Cheng, J.; Zhu, J. Tunable asymmetric acoustic transmission via binary metasurface and zero-index metamaterials. *Appl. Phys. Lett.* **2021**, *118*, 113501. [CrossRef]
20. Fakheri, M.H.; Rajabalipanah, H.; Abdolali, A. Spatiotemporal Binary Acoustic Metasurfaces. *Phys. Rev. Appl.* **2021**, *16*, 024062. [CrossRef]
21. Cao, W.K.; Zhang, C.; Wu, L.T.; Guo, K.Q.; Ke, J.C.; Cui, T.J.; Cheng, Q. Tunable acoustic metasurface for three-dimensional wave manipulations. *Phys. Rev. Appl.* **2021**, *15*, 024026. [CrossRef]
22. Zhu, Y.; Merkel, A.; Donda, K.; Fan, S.; Cao, L.; Assouar, B. Nonlocal acoustic metasurface for ultrabroadband sound absorption. *Phys. Rev. B* **2021**, *103*, 064102. [CrossRef]
23. Ji, J.; Li, D.; Li, Y.; Jing, Y. Low-frequency broadband acoustic metasurface absorbing panels. *Front. Mech. Eng.* **2020**, *6*, 94. [CrossRef]
24. Shen, C.; Xie, Y.; Sui, N.; Wang, W.; Cummer, S.A.; Jing, Y. Broadband acoustic hyperbolic metamaterial. *Phys. Rev. Lett.* **2015**, *115*, 254301. [CrossRef] [PubMed]
25. Shen, C.; Xie, Y.; Li, J.; Cummer, S.A.; Jing, Y. Asymmetric acoustic transmission through near-zero-index and gradient-index metasurfaces. *Appl. Phys. Lett.* **2016**, *108*, 223502. [CrossRef]
26. Gao, H.; Xue, H.; Gu, Z.; Liu, T.; Zhu, J.; Zhang, B. Non-Hermitian route to higher-order topology in an acoustic crystal. *Nat. Commun.* **2021**, *12*, 1888. [CrossRef]
27. Gu, Z.; Gao, H.; Cao, P.C.; Liu, T.; Zhu, X.F.; Zhu, J. Controlling sound in non-hermitian acoustic systems. *Phys. Rev. Appl.* **2021**, *16*, 057001. [CrossRef]
28. Zheng, Y.; Liang, S.; Fan, H.; An, S.; Gu, Z.; Gao, H.; Liu, T.; Zhu, J. Acoustic Luneburg lens based on a gradient metasurface for spoof surface acoustic waves. *JASA Express Lett.* **2022**, *2*, 024004. [CrossRef]
29. Li, Y.; Liang, B.; Gu, Z.M.; Zou, X.Y.; Cheng, J.C. Reflected wavefront manipulation based on ultrathin planar acoustic metasurfaces. *Sci. Rep.* **2013**, *3*, 2546. [CrossRef]
30. Zhao, J.; Li, B.; Chen, Z.; Qiu, C.W. Manipulating acoustic wavefront by inhomogeneous impedance and steerable extraordinary reflection. *Sci. Rep.* **2013**, *3*, 2537. [CrossRef]
31. Zhang, J.; Su, X.; Liu, Y.; Zhao, Y.; Jing, Y.; Hu, N. Metasurface constituted by thin composite beams to steer flexural waves in thin plates. *Int. J. Solids Struct.* **2019**, *162*, 14–20. [CrossRef]
32. Li, Y.; Shen, C.; Xie, Y.; Li, J.; Wang, W.; Cummer, S.A.; Jing, Y. Tunable asymmetric transmission via lossy acoustic metasurfaces. *Phys. Rev. Lett.* **2017**, *119*, 035501. [CrossRef] [PubMed]
33. Zhang, S.; Xia, C.; Fang, N. Broadband acoustic cloak for ultrasound waves. *Phys. Rev. Lett.* **2011**, *106*, 024301. [CrossRef] [PubMed]
34. Zhu, X.; Liang, B.; Kan, W.; Zou, X.; Cheng, J. Acoustic cloaking by a superlens with single-negative materials. *Phys. Rev. Lett.* **2011**, *106*, 014301. [CrossRef] [PubMed]
35. Jiang, X.; Liang, B.; Zou, X.Y.; Yin, L.L.; Cheng, J.C. Broadband field rotator based on acoustic metamaterials. *Appl. Phys. Lett.* **2014**, *104*, 083510. [CrossRef]
36. Kan, W.; Liang, B.; Li, R.; Jiang, X.; Zou, X.Y.; Yin, L.L.; Cheng, J. Three-dimensional broadband acoustic illusion cloak for sound-hard boundaries of curved geometry. *Sci. Rep.* **2016**, *6*, 36936. [CrossRef] [PubMed]
37. Gao, H.; Zhu, Y.F.; Fan, X.D.; Liang, B.; Yang, J.; Cheng, J.C. Non-blind acoustic invisibility by dual layers of homogeneous single-negative media. *Sci. Rep.* **2017**, *7*, 42533. [CrossRef]
38. Jin, Y.; Fang, X.; Li, Y.; Torrent, D. Engineered diffraction gratings for acoustic cloaking. *Phys. Rev. Appl.* **2019**, *11*, 011004. [CrossRef]
39. Zhu, Y.; Hu, J.; Fan, X.; Yang, J.; Liang, B.; Zhu, X.; Cheng, J. Fine manipulation of sound via lossy metamaterials with independent and arbitrary reflection amplitude and phase. *Nat. Commun.* **2018**, *9*, 1632. [CrossRef] [PubMed]
40. Melde, K.; Mark, A.G.; Qiu, T.; Fischer, P. Holograms for acoustics. *Nature* **2016**, *537*, 518–522. [CrossRef]
41. Jiang, X.; Li, Y.; Liang, B.; Cheng, J.C.; Zhang, L. Convert acoustic resonances to orbital angular momentum. *Phys. Rev. Lett.* **2016**, *117*, 034301. [CrossRef]
42. Torrent, D. Acoustic anomalous reflectors based on diffraction grating engineering. *Phys. Rev. B* **2018**, *98*, 060101. [CrossRef]

43. Packo, P.; Norris, A.N.; Torrent, D. Inverse grating problem: Efficient design of anomalous flexural wave reflectors and refractors. *Phys. Rev. Appl.* **2019**, *11*, 014023. [CrossRef]
44. Fu, Y.; Cao, Y.; Xu, Y. Multifunctional reflection in acoustic metagratings with simplified design. *Appl. Phys. Lett.* **2019**, *114*, 053502. [CrossRef]
45. Fu, Y.; Shen, C.; Cao, Y.; Gao, L.; Chen, H.; Chan, C.T.; Cummer, S.A.; Xu, Y. Reversal of transmission and reflection based on acoustic metagratings with integer parity design. *Nat. Commun.* **2019**, *10*, 2326. [CrossRef]
46. Hou, Z.; Fang, X.; Li, Y.; Assouar, B. Highly efficient acoustic metagrating with strongly coupled surface grooves. *Phys. Rev. Appl.* **2019**, *12*, 034021. [CrossRef]
47. Chiang, Y.K.; Oberst, S.; Melnikov, A.; Quan, L.; Marburg, S.; Alù, A.; Powell, D.A. Reconfigurable acoustic metagrating for high-efficiency anomalous reflection. *Phys. Rev. Appl.* **2020**, *13*, 064067. [CrossRef]
48. Fang, X.; Gerard, N.J.; Zhou, Z.; Ding, H.; Wang, N.; Jia, B.; Deng, Y.; Wang, X.; Jing, Y.; Li, Y. Observation of higher-order exceptional points in a non-local acoustic metagrating. *Commun. Phys.* **2021**, *4*, 271. [CrossRef]
49. Packo, P.; Norris, A.N.; Torrent, D. Metaclusters for the full control of mechanical waves. *Phys. Rev. Appl.* **2021**, *15*, 014051. [CrossRef]
50. Bacigalupo, A.; Gnecco, G.; Lepidi, M.; Gambarotta, L. Machine-learning techniques for the optimal design of acoustic metamaterials. *J. Optim. Theory Appl.* **2020**, *187*, 630–653. [CrossRef]
51. Zheng, B.; Yang, J.; Liang, B.; Cheng, J.C. Inverse design of acoustic metamaterials based on machine learning using a Gauss–Bayesian model. *J. Appl. Phys.* **2020**, *128*, 134902. [CrossRef]
52. Wu, R.T.; Liu, T.W.; Jahanshahi, M.R.; Semperlotti, F. Design of one-dimensional acoustic metamaterials using machine learning and cell concatenation. *Struct. Multidiscip. Optim.* **2021**, *63*, 2399–2423. [CrossRef]
53. Gurbuz, C.; Kronowetter, F.; Dietz, C.; Eser, M.; Schmid, J.; Marburg, S. Generative adversarial networks for the design of acoustic metamaterials. *J. Acoust. Soc. Am.* **2021**, *149*, 1162–1174. [CrossRef] [PubMed]
54. Ding, H.; Fang, X.; Jia, B.; Wang, N.; Cheng, Q.; Li, Y. Deep learning enables accurate sound redistribution via nonlocal metasurfaces. *Phys. Rev. Appl.* **2021**, *16*, 064035. [CrossRef]
55. Donda, K.; Zhu, Y.; Merkel, A.; Fan, S.W.; Cao, L.; Wan, S.; Assouar, B. Ultrathin acoustic absorbing metasurface based on deep learning approach. *Smart Mater. Struct.* **2021**, *30*, 085003. [CrossRef]
56. Ahmed, W.W.; Farhat, M.; Zhang, X.; Wu, Y. Deterministic and probabilistic deep learning models for inverse design of broadband acoustic cloak. *Phys. Rev. Res.* **2021**, *3*, 013142. [CrossRef]
57. Wu, R.T.; Jokar, M.; Jahanshahi, M.R.; Semperlotti, F. A physics-constrained deep learning based approach for acoustic inverse scattering problems. *Mech. Syst. Signal Process.* **2022**, *164*, 108190. [CrossRef]
58. Gor'kov, L.P. On the forces acting on a small particle in an acoustical field in an ideal fluid. *Sov. Phys. Dokl.* **1962**, *6*, 773–775.
59. Fan, X.D.; Zhang, L.K. Trapping Force of Acoustical Bessel Beams on a Sphere and Stable Tractor Beams. *Phys. Rev. Appl.* **2019**, *11*, 014055. [CrossRef]
60. Fan, X.D.; Zhang, L. Phase shift approach for engineering desired radiation force: Acoustic pulling force example. *J. Acoust. Soc. Am.* **2021**, *150*, 102–110. [CrossRef]